Applied Catalysis B: Environmental 248 (2019) 184–192

Contents lists available at ScienceDirect

Applied Catalysis B: Environmental

journal homepage: www.elsevier.com/locate/apcatb

Metal-free g-C_3N_4 photocatalysis of organic micropollutants in urban wastewater under visible light

Nuno F.F. Moreira, Maria J. Sampaio*, Ana R. Ribeiro, Cláudia G. Silva, Joaquim L. Faria, Adrián M.T. Silva

Laboratory of Separation and Reaction Engineering – Laboratory of Catalysis and Materials (LSRE-LCM), Departamento de Engenharia Química, Faculdade de Engenharia, Universidade do Porto, Rua Dr. Roberto Frias s/n, 4200-465 Porto, Portugal

ARTICLE INFO

Keywords:
g-C_3N_4
LED
Visible light
Urban wastewater
Organic contaminants
Phytotoxicity

ABSTRACT

Heterogeneous photocatalysis under visible light was employed for the degradation of organic micropollutants (MPs) found in the biologically treated effluents of an urban wastewater treatment plant (UWWTP). The irradiation source consisted in 4 light emitting diodes (LEDs) with a nominal power of 400–500 W m^{-2} at 417 nm. Metal-free exfoliated graphitic carbon nitride (gCN_T), which was synthetized through a simple thermal treatment using dicyandiamide as precursor, was employed as photocatalyst. The gCN_T material was characterized using different techniques: N_2 adsorption isotherms at 77 K, electron microscopy (scanning and transmission) and diffuse reflectance UV–Vis. The photocatalytic performance of the material was compared to the commercial TiO_2-P25, confirming that gCN_T led to a remarkable higher removal efficiency of the target MPs. Most of these MPs were removed in less than 10 min to levels below the limit of quantification (carbamazepine > isoproturon > clopidogrel > diclofenac > atenolol > bezafibrate > tramadol > venlafaxine > fluoxetine). Indirect photolysis, resulting from the secondary reactive oxidants generated during the irradiation of the aqueous matrix components, was found to partially contribute for the elimination of the occurring MPs. In addition, the gCN_T photocatalyst was immobilized on glass rings for use under continuous mode operation, a minimum residence time of 25 min being required to attain significant removal efficiencies. Phytotoxicity experiments showed that heterogeneous photocatalysis did not enhance the toxicity of the wastewaters.

1. Introduction

Organic micropollutants (MPs) are frequently found in the aquatic environment at concentrations levels between ng L^{-1} and μg L^{-1}. The difficult elimination of MPs by physicochemical and biological treatments conventionally applied in the urban wastewater treatment plants (UWWTPs) triggers the need of alternative approaches to remove them. Although discharge limits are not yet regulated for MPs, some recommendations have been launched by European Union (EU) in order to monitor harmful substances, namely the Directive 2013/39/EU [1], which indicates a group of 45 priority substances/groups of substances and recommends new treatment strategies, and the Decision 2015/495/EU [2], setting a Watch List of 17 contaminants of emerging concern (CECs) for EU-monitoring, which was very recently repealed by a new Watch List of 15 CECs [3].

Novel treatment tools have been sought such as advanced oxidation processes (AOPs), which have been largely studied to reach high degradation rates of MPs from UWWTP effluents [4]. However, only UV (mainly for disinfection) and ozonation have been implemented so far at full-scale [5–7], both approaches presenting some limitations but affordable costs when compared with most AOPs. Solar applications of heterogeneous photocatalysis are an interesting alternative to degrade a broad range of MPs [8]. Wide-bandgap optical semiconductors able to act as visible light photocatalysts require absorption edges above the UV limit since this only accounts for less than 5% of the solar spectrum reaching Earth's surface. Visible-light photocatalysts with a narrower bandgap, such as graphitic carbon nitride (g-C_3N_4 with a bandgap of 2.7 eV, corresponding to an absorption edge at 459 nm), have been receiving an increasing interest for a wide variety of photocatalytic applications (*e.g.*, CO_2 and NO_x reduction, degradation of organic pollutants, organic selective synthesis, hydrogen production and water splitting) [9–18]. The high photocatalytic activity of g-C_3N_4 materials on the degradation of different types of organic contaminants in water has been already demonstrated in previous studies, namely for methylene blue [19–22], rhodamine B [22–25], methyl orange [26–28], basic fuchsin, malachite green and crystal violet [29], acid orange 7

* Corresponding author.
E-mail address: mjsampaio@fe.up.pt (M.J. Sampaio).

https://doi.org/10.1016/j.apcatb.2019.02.001
Received 7 August 2018; Received in revised form 24 November 2018; Accepted 1 February 2019
Available online 04 February 2019

[30], oxalic acid [31], tetracycline [32,33], phenol [34–36], atrazine [35,37], carbamazepine and sulfamethoxazole [35,38] and humic acids [39]. However, in the majority of these reports, the experiments are often carried out using ultrapure water, concentrations higher than those usually found in the environment, slurry (batch) systems, metal loaded g-C_3N_4 materials, and spiked matrices [40]. To the best of our knowledge, none of these studies report the treatment of an actual urban wastewater (*i.e.*, not spiked) employing g-C_3N_4 as metal-free photocatalyst.

g-C_3N_4 has been synthesized by thermal polymerization of several nitrogen-rich precursors, namely urea, thiourea, cyanamide, dicyandiamide or melamine [17,41]. Since its photocatalytic activity is struggled by the low surface area and by the fast recombination of electrons and holes, several approaches have been used to overcome these drawbacks, namely the chemical, mechanical and thermal exfoliation treatments of g-C_3N_4 [17,42]. Other procedures include the design of g-C_3N_4 based nanoarchitectures using templating approaches, doping with metals, and modification with other semiconductors, well discussed in the literature [41].

The chemical and thermal stability of the low-cost, metal-free g-C_3N_4 turns this visible light photocatalyst an outstanding option for solar-driven photocatalysis [9,43]. In addition, energy-efficient and low-cost visible light emitting diodes (LEDs) with a narrow emission band can be employed as light sources, as replacement of xenon or mercury lamps, and matching the absorption peak of the material for the economy of the process [43].

The novelty of the present study relies on the application of a highly-efficient photocatalytic process based on a metal-free g-C_3N_4 photocatalyst with enhanced activity towards degradation of a wide range of MPs in realistic urban wastewaters, by using a low-cost and energy-efficient visible light source (LED). The photocatalytic treatment was also performed in continuous mode, by employing an innovative approach with g-C_3N_4-coated glass rings. The phytotoxicity of the wastewater was evaluated, before and after photocatalytic treatment, to infer about the potential formation of reaction by-products toxic for plants, which could compromise water reuse. To the best of our knowledge, this is the first study on heterogeneous photocatalysis using g-C_3N_4 as a semiconductor for the removal of MPs in actual UWWTP effluents.

2. Materials and methods

2.1. Chemicals and materials

Dicyandiamide (99%) supplied from Sigma-Aldrich was used as precursor in the preparation of the bulk g-C_3N_4. Aeroxide® TiO_2-P25 (~80% anatase:20% rutile) powder was supplied by Evonik. Polyvinyl alcohol (PVA), reference standards for liquid chromatography (> 98%) and surrogate standards were purchased from Sigma–Aldrich, which include atenolol, bezafibrate, carbamazepine, clopidogrel, diclofenac, fluoxetine, isoproturon, tramadol venlafaxine, azithromycin-d3, atrazine–d5, diclofenac-d4 and fluoxetine–d5. Ethanol (99.5%) and 2-propanol (100%) were obtained from Fisher Scientific UK Limited. Acetonitrile (MS grade) was supplied by Panreac AppliChem. Formic (99.5%) and sulfuric (98%) acids were acquired from Merck (Darmstadt, Germany). Ultrapure water was produced in a Milli-Q water system (resistivity of 18.2 MΩ cm, at 25 °C). The Oasis® HLB (Hydrophilic-Lipophilic-Balanced) cartridges (150 mg, 6 mL) used for sample preparation, were purchased from Waters (Milford, MA, USA).

2.2. Catalysts preparation and characterization

The bulk g-C_3N_4 material was prepared by thermal decomposition of dicyandiamide, as previously described [17]. Briefly, a certain amount of dicyandiamide precursor was placed in a covered crucible and then heated to 550 °C in air atmosphere for 4 h. In a second step, thermal oxidative exfoliation of the bulk material was conducted at 500 °C. The resulting material was labelled as gCN_T. TiO_2 was used as received, for comparison purposes.

The specific surface area (S_{BET}) of the mentioned photocatalysts was calculated by using the Brunauer-Emmett-Teller (BET) method and N_2 adsorption isotherms obtained at −196 °C in a Quantachrome NOVA 4200e apparatus. The optical absorption was determined in the 220–800 nm range by diffuse reflectance UV–Vis (DRUV-Vis) in a JASCO V-560 spectrophotometer equipped with an integrating sphere. The results were recorded to equivalent absorption Kubelka–Munk units and used to obtain the optical bandgap.

Uncoated glass rings (diameter = 3 mm, length = 3 mm) were cleaned with an anionic detergent in water, under sonication. The washed rings were then immersed in 2-propanol and sonicated for 15 min. Before coating with gCN_T, the glass rings were immersed in a 2% (w/V) aqueous solution of PVA by dip-coating. This procedure was immediately followed by a second dip-coating immersion of the glass rings in a 5% (w/V) gCN_T:ethanol suspension, previously sonicated for 30 min.

The surface morphology of bulk g-C_3N_4, gCN_T powders and gCN_T immobilized on glass rings was observed by scanning electron microscopy (SEM), using a FEI Quanta 400FEG ESEM/EDAX Genesis X4 M instrument. In the case of the immobilized gCN_T, the SEM apparatus was equipped with a sample holder, in which the broken glass rings were positioned to observe and measure the cross-section of the coated material, by using the respective SEM instrument software. Transmission electron microscopy (TEM) was performed on a JEM 220FS microscope (Jeol, Japan) with a LaB6 electron gun operating at 200 kV.

2.3. Experimental set-up

Wastewater samples from the secondary biological treatment of a UWWTP located in the North region of Portugal, were collected and separated in aliquots which were stored at – 4 °C. The photocatalytic performance of the gCN_T powder was studied in batch mode, using a borosilicate reactor containing 60 mL of UWWTP effluent, equipped with four high-power visible LEDs (λ_{max} = 417 nm, Full-Width Half-Maximum (FWHM) = 18.2 nm) perpendicularly placed to each other and equidistant (4.0 cm) from the reactor (Scheme 1a). The nominal irradiation of each LED varied between 400–500 W m^{-2}, as determined by UV-Vis spectroradiometry (USB2000+, OceanOptics, USA). The catalyst load was fixed at 1.0 g L^{-1} (selected in preliminary studies as optimal gCN_T load for the degradation of model organic pollutants). A dark period of 30 min was performed to establish the adsorption-desorption equilibrium under oxygenated conditions (air). Under these conditions, the removals of the 9 studied MPs never exceeded 6% after 30 min of adsorption period with either TiO_2 or gCN_T. Then, the suspension containing the UWWTP effluent and the photocatalyst was irradiated for 60 min, and samples were withdrawn regularly from the reactor.

Photolysis experiments were performed in UWWTP effluent and also in ultrapure water spiked with the MPs found in the UWWTP effluent and at similar concentrations, in this case under air and deoxygenated (argon) conditions. For that, the required volumes of each standard solution were added to a volumetric flask and the organic solvent was evaporated before filling it with the ultrapure water, avoiding the presence of the organic solvent and its possible scavenging effect. Control experiments using ultrapure water as matrix were also run in the dark, under oxygenated and deoxygenated conditions. All the experiments were carried out in triplicate.

Continuous flow experiments were performed using the gCN_T material immobilized on glass rings (Scheme 1b). A borosilicate cylindrical reactor (internal diameter = 2.7 cm, length = 7.0 cm) was packed with 115 gCN_T-coated glass rings. The filling volume after packing was approximately 31.5 mL. The reactor was continuously filled with UWWTP

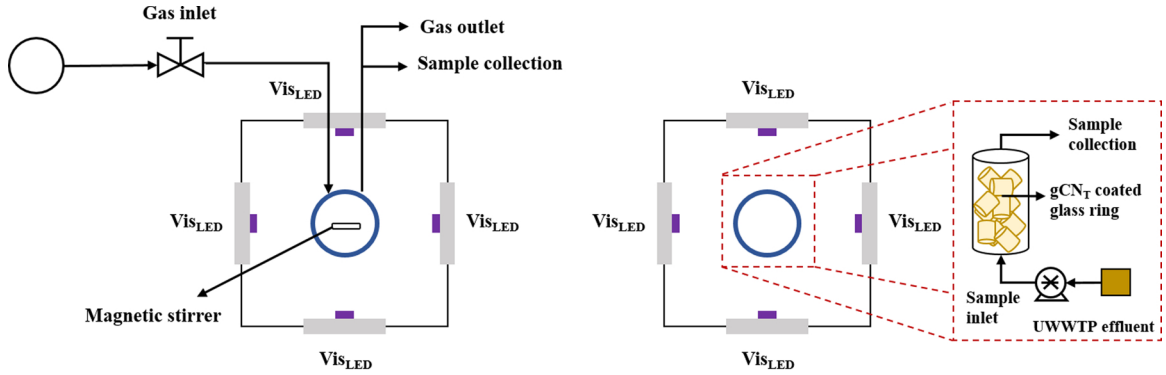

Scheme 1. Photocatalytic experimental set-up under batch (a) and continuous (b) operation modes.

effluent using a peristaltic pump at constant flow rate (Q), and LEDs were then turned on after establishment of the adsorption-desorption equilibrium. Samples were regularly withdrawn after reaching the steady state. Different residence times (2, 5, 12, 25, 55 min) were tested, by changing the liquid flow rate (0.57, 1.26, 2.6, 6.3, 15.7 mL min^{-1}). Uncoated glass rings were used for photolysis experiments (residence time of 55 min) to maintain the hydrodynamic behaviour and light diffusion conditions, allowing the comparison with the photocatalytic experiments.

2.4. Analytical methods

The concentration of each organic MP in the UWWTP effluent was determined by ultra-high performance liquid chromatography with tandem mass spectrometry (UHPLC-MS/MS) in a Shimadzu Corporation apparatus (Tokyo, Japan), consisting of a UHPLC equipment (Nexera) with two pumps (LC-30AD), an autosampler (SIL-30AC), an oven (CTO-20AC), a degasser (DGU-20 A 5R) and a system controller (CBM-20 A) with proper software (LC Solution Version 5.41SP1), coupled to a triple quadrupole mass spectrometer detector (Ultra-Fast Mass Spectrometry series LCMS-8040). Before UHPLC-MS analysis, a pre-concentration and clean up procedure was performed by solid phase extraction (SPE), adding isotopically labeled internal standards to the samples before SPE as described elsewhere [44]. A Cortecs™ C18 + column (100 × 2.1 mm i.d.; 1.6 µm particle diameter), supplied by Waters (Milford, MA, USA), was used with a mobile phase composed by ultrapure water and acetonitrile (20:80, *v/v*), both acidified with 0.1% formic acid. The chromatographic analytical method was performed at isocratic mode, using a flow rate of 0.3 mL min^{-1} and the column oven temperature set at 30 °C. The autosampler temperature was set at 4 °C and the injection volume was 5 µL. For quantification purposes, the selected reaction monitoring (SRM) transition between the precursor ion and the most abundant fragment ion was determined; whereas the second most intense fragment ion was used for confirmation of the identity of each target MP (SRM1/SRM2 ratio).

The dissolved organic carbon (DOC) was determined using a Shimadzu TOC-L apparatus (Shimadzu Scientific Instruments, Japan).

2.5. Phytotoxicity evaluation

PHYTOTOXKIT microbiotests (MicroBioTests Inc.) were used to assess the phytotoxicity, by comparing the germination of the seeds of 3 given plant species, as well as their root and shoot lengths, after exposure during 72 h to distilled water, non-treated and treated UWWTP effluents (after 10 and 60 min using TiO_2 and gCN_T-photocatalysts). The PHYTOTOXKIT microbiotest strictly adheres to ISO standard 18763. The plants were monocotyl *Sorghum saccharatum* (Sorgho), dicotyls *Lepidium sativum* (garden cress) and *Sinapis alba* (mustard). The measurements of root and shoot lengths were performed by image analysis using ImageJ® software (NIH, USA).

3. Results and discussion

3.1. Photocatalyst characterization

The characterization of the bulk g-C_3N_4 and gCN_T materials was presented in our previous work [45] (labeled as bulk and T500, respectively), studying its use for the photocatalytic synthesis of benzaldehyde. In the present work, the most relevant characterization for interpretation of the results was selected, and additional data on the gCN_T immobilized on glass rings before and after the photocatalytic reactions, was included. Briefly, the S_{BET} of the bulk g-C_3N_4 material prepared by direct pyrolysis of dicyandiamide is typically low around ~10 $m^2 g^{-1}$, as experimentally determined. However, after thermal post-treatment at 500 °C, the S_{BET} of the resulting material, gCN_T, increased by *ca.* 12 times to 117 $m^2 g^{-1}$. As already described in the literature, oxidation treatment under air atmosphere may lead to unstable structures, due to the low resilience of the hydrogen bonding between strands of polymeric melon by NH or NH_2 groups [41]. The procedure adopted in this work may promote the gradual exfoliation of the bulk material, due to layer-by-layer thermal oxidation and splitting, resulting in a higher S_{BET} [46,47]. For comparison purposes, the S_{BET} determined for TiO_2 was 54 $m^2 g^{-1}$.

The DRUV-Vis spectrum of gCN_T, shows an unresolved broad band fading out between 450 and 500 nm (Fig. 1). It is significantly shifted to the red region leading to a higher light absorption range through the

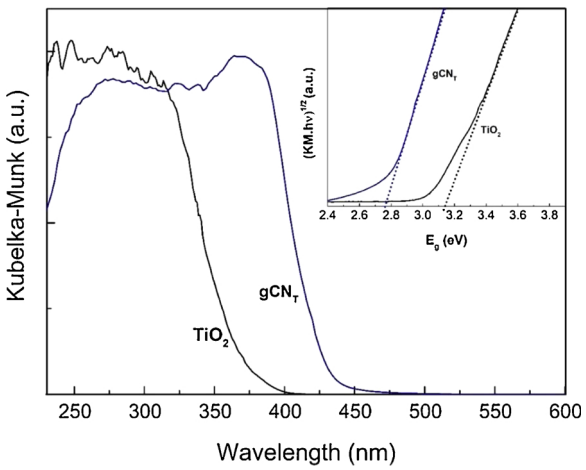

Fig. 1. DRUV-Vis spectra of TiO_2 and gCN_T photocatalysts; inset: plot of Kubelka-Munk units as a function of the light energy.

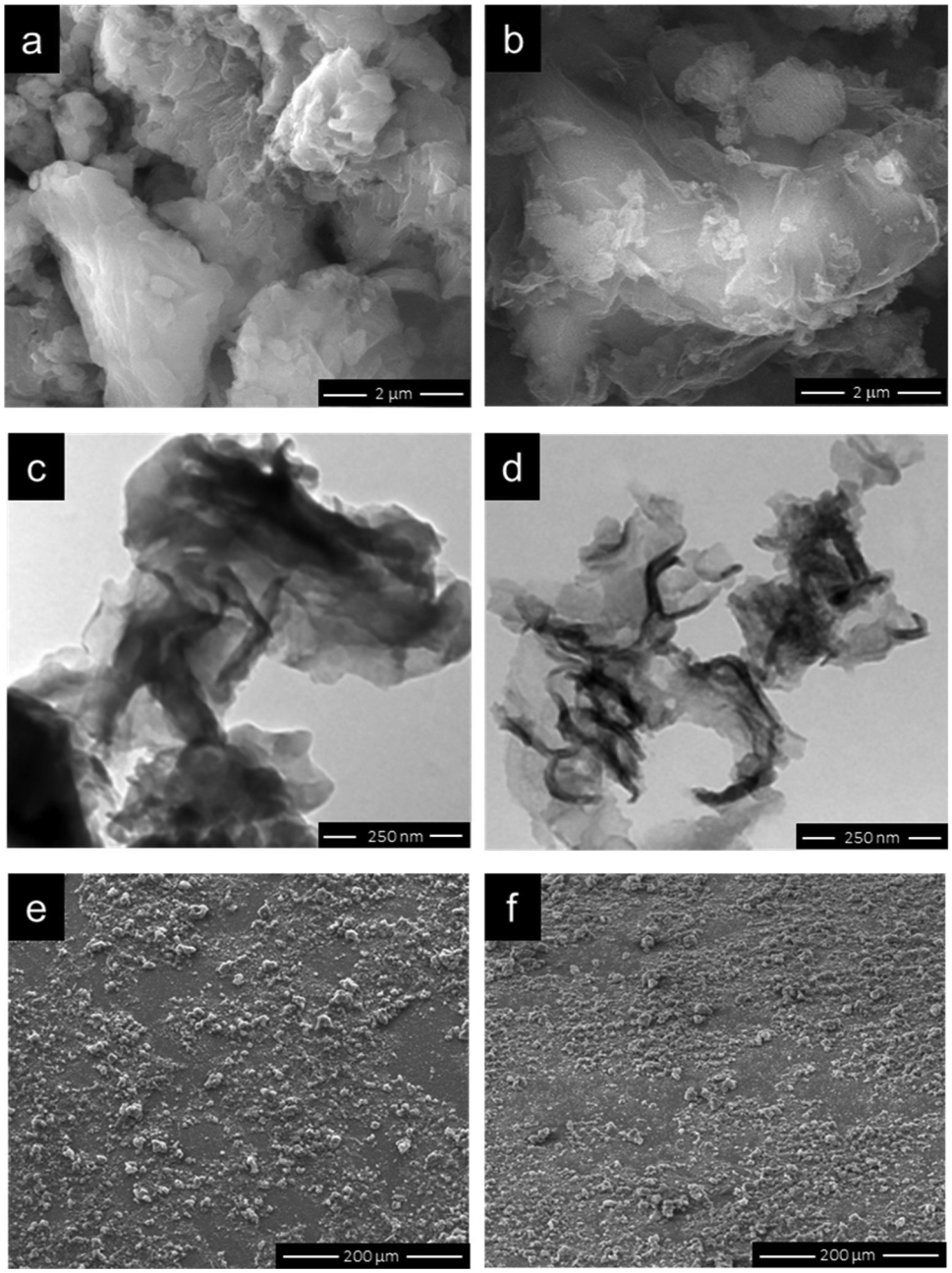

Fig. 2. SEM (a, b) and TEM (c, d) images of bulk g-C_3N_4 (a, c) and gCN_T (b, d) powder materials. SEM of gCN_T immobilized on glass rings before (e) and after (f) usage in the photocatalytic reactions.

visible spectrum, in comparison to TiO_2. The commercial TiO_2 photocatalyst shows the characteristic absorption band sharp edge rising at 400 nm. The bandgap energies (E_g) of both photocatalysts were estimated by the Tauc plot (inset Fig. 1), using the equivalent absorption Kubelka-Munk (*KM*) units of the absorption edges, $(KM.h.\nu)^{1/2}$ versus E_g, where h is Plank' constant and ν is the light frequency. The E_g determined for TiO_2 and gCN_T were 3.14 and 2.76 eV, respectively.

The morphology of bulk g-C_3N_4 and gCN_T materials was assessed by SEM and TEM micrographs (Fig. 2), revealing differences in their morphology.

The bulk material is constituted by g-C_3N_4 sheets assembled in dense aggregates (SEM, Fig. 2a), resulting from the stacking of the layers. In the case of gCN_T (SEM, Fig. 2b), thinner plates surrounded by small aggregates of non-exfoliated g-C_3N_4 material were observed, resulting from the progressive oxidation of the hydrogen bonds between the layers, *i.e.* the exfoliation originated by the thermal oxidation treatment, in agreement with the results obtained from S_{BET} measurements. TEM analysis of the materials was also performed (Fig. 2c and 2d) and the results corroborate with those given before, less dense layers being observed in the case of the gCN_T material. A representative SEM micrograph of the fresh gCN_T coated glass rings reveals its regular distribution over the support (Fig. 2e). These gCN_T coated glass rings were analyzed after being employed in the photocatalytic treatment of the UWWTP effluent, under continuous mode and during several hours, the morphology remaining uniform and, thus, confirming their stability under the tested conditions (Fig. 2f).

3.2. Degradation of MPs in batch mode using powder photocatalysts

The photochemical degradation of a set of 9 organic MPs quantified in the UWWTP effluent was carried out in the absence of catalyst by irradiating at 417 nm using LEDs as light source (Fig. 3). Under these

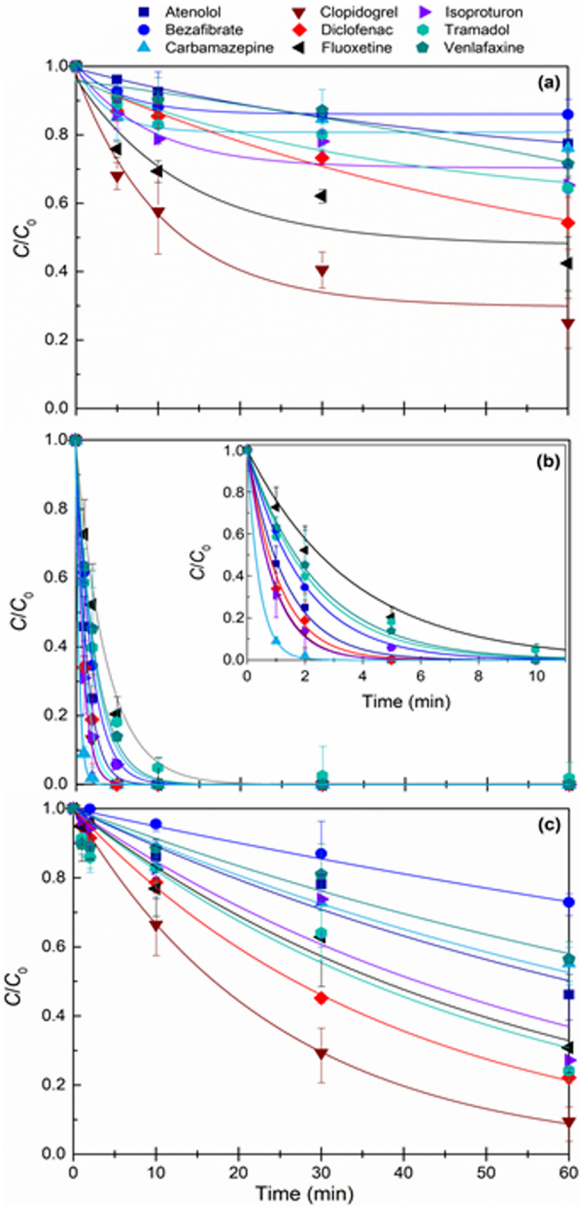

Fig. 3. Normalized concentration of the MPs (C/C_0) identified in the UWWTP effluents, after treatment by photolysis (a), and by heterogeneous photocatalysis using gCN_T (b) and TiO_2 (c). Experiments were performed in batch mode (60 mL) and with four LEDs, using a catalyst load of 1.0 g L^{-1}. LEDs were switched on after a dark period of 30 min to establish the adsorption-desorption equilibrium.

conditions, a surprisingly significant abatement of the MPs (clopidogrel > fluoxetine > diclofenac > isoproturon ≈ tramadol ≈ venlafaxine > carbamazepine ≈ atenolol > bezafibrate) was observed (Fig. 3a). This occurrence could not arise from direct single photon absorption since none of the target compounds will absorb on the emission band of the LED (Fig. S1). However, indirect photolysis may take place by irradiation of the nitrates naturally present in UWWTP effluents (~0.40 mg L^{-1} in this particular case, Table S1): nitrate photochemistry gives raise to reactive oxygen species (ROS), namely singlet oxygen ($^1O_2$), hydroxyl radicals ($HO^•$) or alkyl peroxyl radicals ($ROO^•$) and hydrated electrons from the ionization of water solvent molecules [48,49]. In addition, photosensitization phenomena may occur by light absorbing species, such as colored organic matter in its triplet state with the ability to break the organic MPs, leading to their indirect photochemical decomposition [48–50]. Less common will be the occurrence of non-linear photon absorption phenomena, such as the simultaneous absorption of two photons [51].

Considering that the complexity of the matrix may affect the degradation kinetics of the MPs [52–54], photolysis experiments were performed using ultrapure water spiked with a solution containing the 9 organic MPs with similar concentrations to those found in the UWWTP effluents, under oxygenated and deoxygenated conditions, and with/without light irradiation. Markedly lower removals were obtained when using ultrapure water as matrix (Fig. S2) instead of the real wastewater (Fig. 3a), and quite similar results were obtained when the solutions were saturated with argon or oxygen, under both dark and light conditions. Thus, photosensitization, indirect photolysis, or other mechanisms involving other matrix species, could take place under visible light driving the degradation of the MPs in the UWWTP effluent.

The photocatalytic degradation of the MPs in the UWWTP effluents followed a pseudo-first order rate law (Fig. 3b and c). The apparent first order reaction rate constants (k_{app}) summarized in Table 1 were determined by exponential curve fitting to the experimental data.

The photocatalytic experiments using the powdered gCN_T led to an almost complete removal of all MPs (carbamazepine > isoproturon > clopidogrel > diclofenac > atenolol > bezafibrate > tramadol > venlafaxine > fluoxetine) after 10 min of reaction (*i.e.*, after turning on the LEDs) (Fig. 3b). It is important to refer that the k_{app} obtained for each MP hold one to three orders of magnitude compared with the TiO_2, proving the high efficiency of this catalyst under the reaction conditions used.

Regarding the standard TiO_2 photocatalyst (Fig. 3c), it is observed that the conversion is only slightly better that the photolytic degradation of the MPs. In addition, a different degradation order of the MPs is observed (clopidogrel > diclofenac > tramadol > fluoxetine > isoproturon > atenolol > carbamazepine > venlafaxine > bezafibrate), when comparing with the gCN_T material. The distinct behaviour observed for both catalysts can be expected, especially by using a real matrix containing naturally occurring interferences that may act as promoters or inhibitors (such as organic matter consuming $HO^•$ radicals and other oxidizing species; anions acting as $HO^•$ scavengers; organic and inorganics species competing for the active reaction sites, etc.). Moreover, the photocatalytic activity of the TiO_2 under the light source used (λ_{max} = 417 nm) can also be explained in terms of the residual overlap between the absorption spectrum of TiO_2 and the emission of the LED (Fig. S3). Obviously, it is not expected that a wide-bandgap optical semiconductor such as TiO_2 (E_g ~ 3.14 eV) would be efficient under 417 nm excitation, since UV-light is required to effectively activate it. Nevertheless, the comparison between the TiO_2 (E_g ~ 3.14 eV) and the gCN_T (E_g ~ 2.76 eV) under visible light was performed based on previous studies using LEDs emitting either in the UV or visible ranges. In those experiments, the performance of both TiO_2 and gCN_T was evaluated on the degradation of diclofenac as model compound (Fig. S4). The results demonstrated that even under UV light, the gCN_T material exhibited better performance compared with TiO_2,

Table 1
Initial concentration (ng L^{-1}) and apparent first order reaction rate constant (k_{app}, min^{-1}) for each MP using different treatment processes.

Compound	Initial concentration (ng L^{-1})	k_{app} ($\times 10^{-2}$ min^{-1})	
		VIS_{LED}/ gCN_T	VIS_{LED}/ TiO_2
Atenolol	12.5 ± 1.2	74.3 ± 2.3	1.2 ± 0.1
Bezafibrate	38.7 ± 6.0	51.9 ± 1.2	0.5 ± 0.0
Carbamazepine	763 ± 18	238 ± 1	1.1 ± 0.2
Clopidogrel	93.2 ± 10.7	108 ± 2	4.1 ± 0.0
Diclofenac	1102 ± 31	90.6 ± 2.6	2.6 ± 0.1
Fluoxetine	21.7 ± 4.5	27.4 ± 4.5	1.9 ± 0.2
Isoproturon	84.6 ± 7.4	110 ± 8	1.7 ± 0.3
Tramadol	3930 ± 244	44.6 ± 3.6	2.0 ± 0.3
Venlafaxine	349 ± 47	41.3 ± 1.2	0.9 ± 0.2

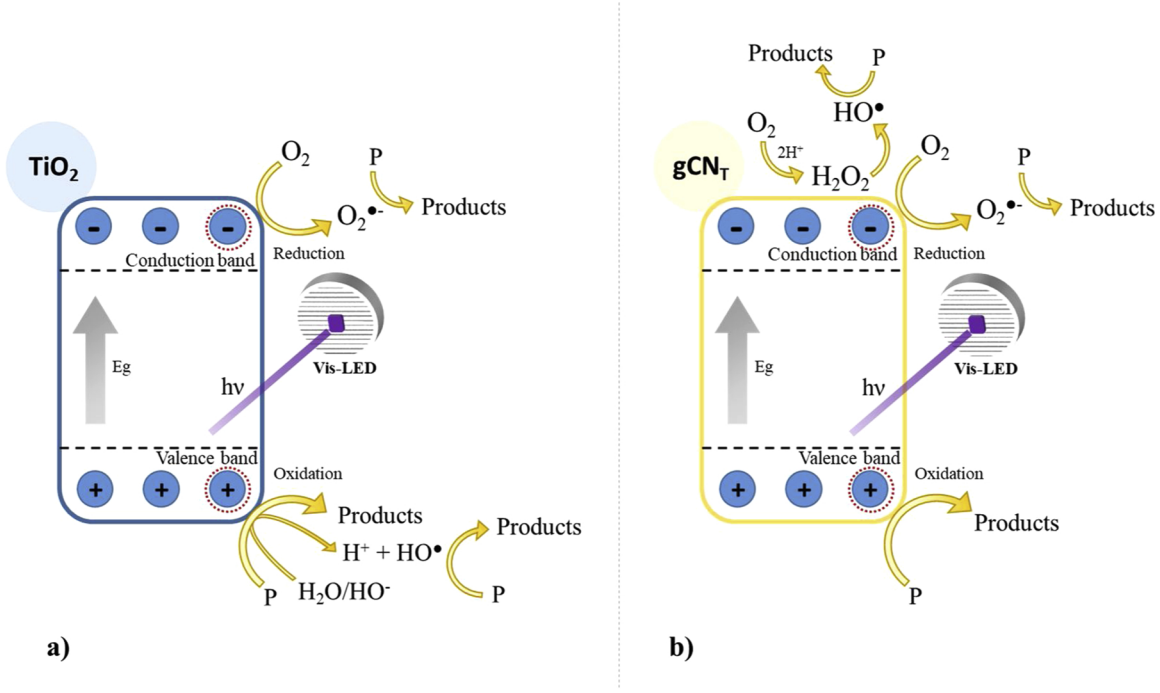

Scheme 2. Schematic representation of a possible photocatalytic mechanism for the degradation of MPs using TiO_2 (a) or gCN_T (b).

showing the high efficiency of gCN_T in both UV and visible ranges.

The efficiency of g-C_3N_4 based photocatalysts to eliminate organic contaminants (mostly dyes) is already known from the literature [19,20,23,24,26,27,29,34,37,39]. In the unique study reported to a spiked effluent from a UWWTP [35], the photocatalytic degradation of four model compounds (phenol, atrazine, sulfamethoxazole and carbamazepine at 100 μM), under visible illumination (xenon lamp; $\lambda > 400$ nm), was attributed to reactive oxygen species and/or contaminant-photocatalyst interfacial interactions, depending on the g-C_3N_4 sample tested. Furthermore, the photocatalytic activity was similar regardless of the realistic matrix tested (water or wastewater), demonstrating the potential of g-C_3N_4 for the treatment of real case effluents.

Scheme 2 shows the possible pathway for gCN_T catalyst compared with the well-known TiO_2 [55], generally based from mechanism studies of model pollutants in aqueous solutions, *i.e.* considering that the others constituents present in the UWWTP effluent (organic matter, nitrates and other inorganics, etc.) do not interfere on the photocatalytic mechanism. However, it is important to remark that the photocatalytic experiments investigating the efficiency of the gCN_T were performed using UWWTP effluent as matrix, which turns the understanding of the mechanisms occurring and governing the degradation pathway at the catalyst surface much more challenging to predict.

Concerning the organic matter, no significant changes on the DOC content of the effluent from the UWWTP were observed before and after the treatment with both photocatalysts. This is not surprisingly due to the complexity of the matrix: there are several orders of magnitude of difference between the concentration of the studied organic MPs (in the range of ng L^{-1} to μg L^{-1}) and the DOC content (in the range of mg L^{-1}).

3.3. Degradation of MPs in continuous mode using gCN_T-coated glass rings

Slurry reactors have as typical disadvantage the need to separate the catalyst from the treated water, in many cases highly energy-consuming processes being required. The immobilization of the photocatalyst on a proper support is seen as a possibility to overcome this drawback in heterogeneous photocatalysis. However, there is a price to pay with immobilization since a decrease in the photocatalytic efficiency must arise from the fact that the reaction mostly occurs at the catalyst-solution interface and a catalyst dispersed in the matrix maximises the contact area [56–58]. The application of continuous mode operating systems, in some cases using immobilized catalysts, was already studied by various authors [57,59–62].

In order to evaluate the feasibility of gCN_T photocatalysis as an option for application in a real case UWWTP, the removal of the target organic MPs of the effluent samples was further studied using the gCN_T immobilized on glass rings, under continuous mode operation. Different residence times (2, 5, 12, 25, 55 min) were tested, as shown in Fig. 4. Control experiments were done conducting the photochemical degradation of the target organic MPs with uncoated glass rings during 55 min of residence time. More significant degrees of removal were found for clopidogrel, fluoxetine and diclofenac, as also observed for photolysis experiments in slurry (*i.e.* batch) mode, reinforcing the idea that other mechanisms besides direct photolysis affected the removal of MPs, namely indirect photolysis, photosensitization and/or photo(hydrolysis).

When the reactor was loaded with gCN_T immobilized on glass rings and, before switching on the LEDs, the UWWTP effluent was passed through the reactor to establish the adsorption-desorption equilibrium, during *ca.* 9 h for the lower flow rate (residence time of 55 min).

Under the photocatalytic process, using gCN_T coated glass rings after approximately 27 h at the highest residence time (55 min), the photocatalyst maintained its activity leading to identical removal efficiencies. Similar results were obtained for the residence times of 25 and 55 min, suggesting that residences times higher than 25 min will not significantly enhance the removal efficiencies of these MPs, probably due to limitations with the effectively irradiated active sites. For lower residence times, these efficiencies decreased, as expected due to the shorter contact between the organic compounds and the semiconductor.

Quite lower removals were obtained in continuous mode operation in comparison with the slurry (batch) system. As an example, nearly complete removal of the MPs was obtained in batch mode after 10 min (Fig. 3b), whereas the following removal efficiencies were obtained in

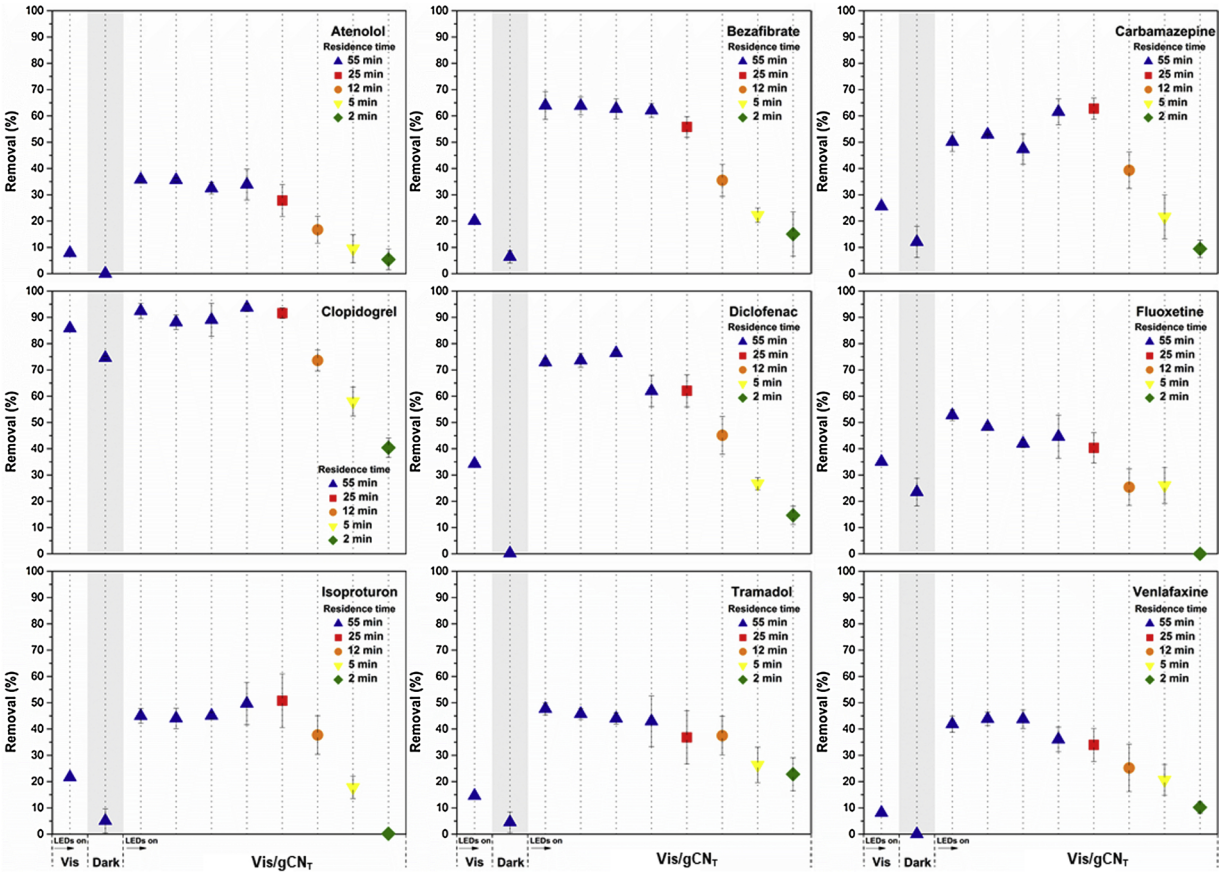

Fig. 4. Removal (%) of the MPs found in UWWTP effluents, after treatment by photolysis, adsorption and photocatalysis using gCN_T immobilized in glass rings under continuous mode operation for different treatment residence times. Experiments were performed in continuous mode (useful volume of 31.5 mL) with four LEDs, packing the reactor with 115 gCN_T-coated glass rings. LEDs were switched on after the adsorption-desorption equilibrium was established (UWWTP effluent was passed through the reactor during ca. 9 h for the lower flow rate (residence time of 55 min)). The samples were withdrawn after the steady state was achieved.

continuous mode for a residence time of 5 min (equivalent treatment time of 10 min in batch mode): atenolol (≈ 10%), bezafibrate (≈ 20%), carbamazepine (≈ 20%), clopidogrel (≈ 60%), diclofenac (≈ 25%), fluoxetine (≈ 20%), isoproturon (≈ 20%), tramadol (≈ 20%) and venlafaxine (≈ 20%). This finding was expected since the catalyst-solution interface decreases when using gCN_T coated glass rings. Again, in what concerns to the amount of organic matter, no significant changes on the DOC content were verified for all the tested residence times, by the same reasons given previously for batch mode. The application of coated-materials requires more treatment time for the effective degradation of pollutants due to the lower area of catalyst per unit of volume, when compared to the use of powder suspensions. However, some practical problems arising from the application of powder photocatalysts are avoided, such as the catalyst separation from the treated water.

The photocatalytic treatment under continuous mode using gCN_T coated glass rings to remove MPs from the effluents of UWWTP is nevertheless possible, but still a challenging technological solution. Further research is needed regarding the optimization of several parameters, such as the length of the column, the amount of catalyst immobilized on the support, the size and number of gCN_T-coated glass rings per unit volume, and the light distribution in the reactor, aiming to increase the process efficiency in continuous mode operation.

3.4. Phytotoxicity measurements

The phytotoxicity was assessed using the PHYTOTOXKIT microbiotest (MicroBioTests Inc.), according to the standard operating protocols for three plant species (*i.e. Sorghum saccharatum, Lepidium sativum* and *Sinapis alba*). The samples from the UWWTP before and after treatment by photocatalysis (using both TiO_2 and gCN_T), did not inhibited the germination of seeds (results not shown).

4. Conclusions

The heterogeneous photocatalysis of MPs in real case effluents of UWWTP was successfully achieved under visible light activation. Among the target MPs found in the UWWTP effluent, the gCN_T photocatalyst showed significantly higher removal rates than the benchmark TiO_2, which can be explained by the suitable E_g and good redox ability of the photogenerated carriers.

Complete removals (to values bellow the limits of quantification) were found in *ca.* 10 min of slurry photocatalytic treatment using gCN_T as catalyst. Moreover, only 5 min were enough to eliminate atenolol, carbamazepine, clopidogrel and diclofenac. As expected, lower efficiencies were observed for the removal of these MPs when the photocatalytic treatment was performed under continuous mode employing gCN_T immobilized on glass rings. Nevertheless, this strategy is important, considering the cost of separation processes and energy requirements for the recovery of the photocatalyst, prior to water reuse or discharge.

The present work showed the potential of gCN_T used in conjunction with visible LEDs to remove several organic MPs present in actual effluents from UWWTP. This can be relevant to the reduction of MPs in UWWTPs, or in other end-of-pipe solutions. It is however clear that parallel to the development of treatment solutions to minimize the impact of MPs on the environment, further optimization is needed.

Acknowledgments

This work is a result of Projects: "AIProcMat@N2020 – Advanced Industrial Processes and Materials for a Sustainable Northern Region of Portugal 2020" (NORTE-01-0145- FEDER-000006), supported by NORTE 2020 (Programa Operacional Regional do Norte), under the Portugal 2020 Partnership Agreement, through the European Regional Development Fund (ERDF); Associate Laboratory LSRE-LCM - UID/EQU/50020/2019 - funded by national funds through FCT (Fundação para a Ciência e a Tecnologia)/MCTES (PIDDAC); POCI-01-0145-FEDER-030674 and POCI-01-0145-FEDER-031398 funded by ERDF through COMPETE2020 - Programa Operacional Competitividade e Internacionalização (POCI) – and by national funds through FCT; and Project NORTE-01-0145-FEDER-031049 funded by ERDF funds through NORTE 2020 and by national funds (PIDDAC) through FCT/MCTES. NFFM acknowledges the research grant from FCT (PD/BD/114318/2016). C.G.S. acknowledges the FCT Investigator Programme (IF/00514/2014) with financing from the European Social Fund (ESF) and the Human Potential Operational Programme. Technical assistance of CEMUP team with SEM analysis is gratefully acknowledged.

Appendix A. Supplementary data

Supplementary material related to this article can be found, in the online version, at doi:https://doi.org/10.1016/j.apcatb.2019.02.001.

References

[1] Directive, Directive 2013/39/EU of the European Parliament and of the Council of 12 August 2013 amending Directives 2000/60/EC and 2008/105/EC as regards priority substances in the field of water policy, Off. J. Eur. Union (2013) 1–17.
[2] Decision_495, Comission implementing Decision (EU) 2015/495 of 20 March 2015 establishing a watch list of substances for Union-wide monitoring in the field of water policy pursuant to Directive 2008/105/EC of the European Parliament and of the Council, Off. J. Eur. Union L 78 (2015) 40–42.
[3] Decision_840, Comission implementing Decision (EU) 2018/840 of 5 June 2018 establishing a watch list of substances for Union-wide monitoring in the field of water policy pursuant to Directive 2008/105/EC of the European Parliament and of the Council and repealing Commission implementing Decision (EU) 2015/495, Off. J. Eur. Union L 141 (2018) 9–12.
[4] A.R. Ribeiro, O.C. Nunes, M.F.R. Pereira, A.M.T. Silva, An overview on the advanced oxidation processes applied for the treatment of water pollutants defined in the recently launched Directive 2013/39/EU, Environ. Int. 75 (2015) 33–51.
[5] J. Hollender, S.G. Zimmermann, S. Koepke, M. Krauss, C.S. McArdell, C. Ort, H. Singer, U. von Gunten, H. Siegrist, Elimination of organic micropollutants in a municipal wastewater treatment plant upgraded with a full-scale post-ozonation followed by sand filtration, Environ. Sci. Technol. 43 (2009) 7862–7869.
[6] F. Itzel, L. Gehrmann, H. Bielak, P. Ebersbach, A. Boergers, H. Herbst, C. Maus, A. Simon, E. Dopp, M. Hammers-Wirtz, T.C. Schmidt, J. Tuerk, Investigation of full-scale ozonation at a municipal wastewater treatment plant using a toxicity-based evaluation concept, J. Toxicol. Environ. Health. Part A 80 (2017) 1242–1258.
[7] I. Silva, M. Tacão, R.D.S. Tavares, R. Miranda, S. Araújo, C.M. Manaia, I. Henriques, Fate of cefotaxime-resistant Enterobacteriaceae and ESBL-producers over a full-scale wastewater treatment process with UV disinfection, Sci. Total Environ. 639 (2018) 1028–1037.
[8] N.F.F. Moreira, C. Narciso-da-Rocha, M.I. Polo-López, L.M. Pastrana-Martínez, J.L. Faria, C.M. Manaia, P. Fernández-Ibáñez, O.C. Nunes, A.M.T. Silva, Solar treatment (H_2O_2, TiO_2-P25 and GO-TiO_2 photocatalysis, photo-Fenton) of organic micropollutants, human pathogen indicators, antibiotic resistant bacteria and related genes in urban wastewater, Water Res. 135 (2018) 195–206.
[9] S. Kumar, S. Karthikeyan, A. Lee, G-C_3N_4-Based nanomaterials for visible light-driven photocatalysis, Catalysts 8 (2018) 74.
[10] L. Cheng, T. Zhang, H. Vo, D. Diaz, D. Quanrud, R.G. Arnold, A.E. Sáez, Effectiveness of engineered and natural wastewater treatment processes for the removal of trace organics in water reuse, J. Environ. Eng. 143 (2017) 03117004.
[11] G. Zhang, Z.-A. Lan, L. Lin, S. Lin, X. Wang, Overall water splitting by Pt/g-C_3N_4 photocatalysts without using sacrificial agents, Chem. Sci. 7 (2016) 3062–3066.
[12] W. Che, W. Cheng, T. Yao, F. Tang, W. Liu, H. Su, Y. Huang, Q. Liu, J. Liu, F. Hu, Z. Pan, Z. Sun, S. Wei, Fast photoelectron transfer in (Cring)–C_3N_4 plane heterostructural nanosheets for overall water splitting, J. Am. Chem. Soc. 139 (2017) 3021–3026.
[13] X. Yuan, C. Zhou, Y. Jin, Q. Jing, Y. Yang, X. Shen, Q. Tang, Y. Mu, A.K. Du, Facile synthesis of 3D porous thermally exfoliated g-C_3N_4 nanosheet with enhanced photocatalytic degradation of organic dye, J. Colloid Interface Sci. 468 (2016) 211–219.
[14] M. Sturini, A. Speltini, F. Maraschi, G. Vinci, A. Profumo, L. Pretali, A. Albini, L. Malavasi, g-C_3N_4-promoted degradation of ofloxacin antibiotic in natural waters under simulated sunlight, Environ. Sci. Pollut. Res. - Int. 24 (2017) 4153–4161.
[15] D. Lu, H. Wang, X. Zhao, K.K. Kondamareddy, J. Ding, C. Li, P. Fang, Highly efficient visible-light-induced photoactivity of Z-scheme g-C_3N_4/Ag/MoS_2 ternary photocatalysts for organic pollutant degradation and production of hydrogen, ACS Sustain. Chem. Eng. 5 (2017) 1436–1445.
[16] M.J. Muñoz-Batista, D. Rodríguez-Padrón, A.R. Puente-Santiago, A. Kubacka, R. Luque, M. Fernández-García, Sunlight-driven hydrogen production using an annular flow photoreactor and g-C_3N_4-Based catalysts, ChemPhotoChem 2 (2018) 870–877.
[17] M.J. Lima, A.M.T. Silva, C.G. Silva, J.L. Faria, Graphitic carbon nitride modified by thermal, chemical and mechanical processes as metal-free photocatalyst for the selective synthesis of benzaldehyde from benzyl alcohol, J. Catal. 353 (2017) 44–53.
[18] K. Cerdan, W. Ouyang, J.C. Colmenares, M.J. Muñoz-Batista, R. Luque, A.M. Balu, Facile mechanochemical modification of g-C_3N_4 for selective photo-oxidation of benzyl alcohol, Chem. Eng. Sci. 194 (2018) 78–84.
[19] J. Liu, T. Zhang, Z. Wang, G. Dawson, W. Chen, Simple pyrolysis of urea into graphitic carbon nitride with recyclable adsorption and photocatalytic activity, J. Mater. Chem. 21 (2011) 14398–14401.
[20] D. Xu, X. Li, J. Liu, L. Huang, Synthesis and photocatalytic performance of europium-doped graphitic carbon nitride, J. Rare Earths 31 (2013) 1085–1091.
[21] H. Zhu, D. Chen, D. Yue, Z. Wang, H. Ding, In-situ synthesis of g-C_3N_4-P25 TiO_2 composite with enhanced visible light photoactivity, J. Nanoparticle Res. 16 (2014) 2632.
[22] X.-j. Wang, W.-y. Yang, F.-t. Li, Y.-b. Xue, R.-h. Liu, Y.-j. Hao, In situ microwave-assisted synthesis of porous N-TiO_2/g-C_3N_4 heterojunctions with enhanced visible-light photocatalytic properties, Ind. Eng. Chem. Res. 52 (2013) 17140–17150.
[23] G. Liao, S. Chen, X. Quan, H. Yu, H. Zhao, Graphene oxide modified g-C_3N_4 hybrid with enhanced photocatalytic capability under visible light irradiation, J. Mater. Chem. 22 (2012) 2721–2726.
[24] X. Song, H. Tao, L. Chen, Y. Sun, Synthesis of Fe/g-C_3N_4 composites with improved visible light photocatalytic activity, Mater. Lett. 116 (2014) 265–267.
[25] Y. Wang, Y. Wang, Y. Li, H. Shi, Y. Xu, H. Qin, X. Li, Y. Zuo, S. Kang, L. Cui, Simple synthesis of Zr-doped graphitic carbon nitride towards enhanced photocatalytic performance under simulated solar light irradiation, Catal. Commun. 72 (2015) 24–28.
[26] S.C. Yan, Z.S. Li, Z.G. Zou, Photodegradation performance of g-C_3N_4 fabricated by directly heating melamine, Langmuir 25 (2009) 10397–10401.
[27] J. Fu, B. Chang, Y. Tian, F. Xi, X. Dong, Novel C_3N_4-CdS composite photocatalysts with organic-inorganic heterojunctions: in situ synthesis, exceptional activity, high stability and photocatalytic mechanism, J. Mater. Chem. A 1 (2013) 3083–3090.
[28] S.M.N. Jeghan, J.Y. Do, M. Kang, Fabrication of flower-like copper cobaltite/graphitic-carbon nitride ($CuCo_2O_4$/g-C_3N_4) composite with superior photocatalytic activity, J. Ind. Eng. Chem. 57 (2018) 405–415.
[29] S. Wang, D. Li, C. Sun, S. Yang, Y. Guan, H. He, Synthesis and characterization of g-C_3N_4/Ag_3VO_4 composites with significantly enhanced visible-light photocatalytic activity for triphenylmethane dye degradation, Appl. Catal. B: Environ. 144 (2014) 885–892.
[30] J. Li, J. Fang, L. Gao, J. Zhang, X. Ruan, A. Xu, X. Li, Graphitic carbon nitride induced activity enhancement of OMS-2 catalyst for pollutants degradation with peroxymonosulfate, Appl. Surf. Sci. 402 (2017) 352–359.
[31] J. Yin, G. Liao, D. Zhu, P. Lu, L. Li, Photocatalytic ozonation of oxalic acid by g-C_3N_4/graphene composites under simulated solar irradiation, J. Photochem. Photobiol. A: Chem. 315 (2016) 138–144.
[32] Y. Deng, L. Tang, G. Zeng, J. Wang, Y. Zhou, J. Wang, J. Tang, L. Wang, C. Feng, Facile fabrication of mediator-free Z-scheme photocatalyst of phosphorous-doped ultrathin graphitic carbon nitride nanosheets and bismuth vanadate composites with enhanced tetracycline degradation under visible light, J. Colloid Interface Sci. 509 (2018) 219–234.
[33] L. Jiang, X. Yuan, G. Zeng, Z. Wu, J. Liang, X. Chen, L. Leng, H. Wang, H. Wang, Metal-free efficient photocatalyst for stable visible-light photocatalytic degradation of refractory pollutant, Appl. Catal. B: Environ. 221 (2018) 715–725.
[34] H.-T. Ren, S.-Y. Jia, Y. Wu, S.-H. Wu, T.-H. Zhang, X. Han, Improved photochemical reactivities of Ag_2O/g-C_3N_4 in phenol degradation under UV and visible light, Ind. Eng. Chem. Res. 53 (2014) 17645–17653.
[35] Q. Zheng, D.P. Durkin, J.E. Elenewski, Y. Sun, N.A. Banek, L. Hua, H. Chen, M.J. Wagner, W. Zhang, D. Shuai, Visible-light-responsive graphitic carbon nitride: rational design and photocatalytic applications for water treatment, Environ. Sci. Technol. 50 (2016) 12938–12948.
[36] L. Tian, J. Li, F. Liang, J. Wang, S. Li, H. Zhang, S. Zhang, Molten salt synthesis of tetragonal carbon nitride hollow tubes and their application for removal of pollutants from wastewater, Appl. Catal. B: Environ. 225 (2018) 307–313.
[37] W.-K. Jo, T. Adinaveen, J.J. Vijaya, N.C. Sagaya Selvam, Synthesis of MoS_2 nanosheet supported Z-scheme TiO_2/g-C_3N_4 photocatalysts for the enhanced photocatalytic degradation of organic water pollutants, RSC Adv. 6 (2016) 10487–10497.
[38] A. Kumar, A. Kumar, G. Sharma, Aa.H. Al-Muhtaseb, M. Naushad, A.A. Ghfar, F.J. Stadler, Quaternary magnetic BiOCl/g-C_3N_4/Cu_2O/Fe_3O_4 nano-junction for visible light and solar powered degradation of sulfamethoxazole from aqueous environment, Chem. Eng. J. 334 (2018) 462–478.
[39] S. Ma, S. Zhan, Y. Jia, Q. Shi, Q. Zhou, Enhanced disinfection application of Ag-modified g-C_3N_4 composite under visible light, Appl. Catal. B: Environ. 186 (2016) 77–87.
[40] B. Xu, M.B. Ahmed, J.L. Zhou, A. Altaee, G. Xu, M. Wu, Graphitic carbon nitride based nanocomposites for the photocatalysis of organic contaminants under visible irradiation: progress, limitations and future directions, Sci. Total Environ. 633 (2018) 546–559.

[41] W.-J. Ong, L.-L. Tan, Y.H. Ng, S.-T. Yong, S.-P. Chai, Graphitic carbon nitride (g-C_3N_4)-Based photocatalysts for artificial photosynthesis and environmental remediation: are we a step closer to achieving sustainability? Chem. Rev. 116 (2016) 7159–7329.
[42] W. Yong, W. Xinchen, A. Markus, Polymeric graphitic carbon nitride as a heterogeneous organocatalyst: from photochemistry to multipurpose catalysis to sustainable chemistry, Angew. Chemie Int. Ed. 51 (2012) 68–89.
[43] L. Svoboda, P. Praus, M.J. Lima, M.J. Sampaio, D. Matýsek, M. Ritz, R. Dvorský, J.L. Faria, C.G. Silva, Graphitic carbon nitride nanosheets as highly efficient photocatalysts for phenol degradation under high-power visible LED irradiation, Mater. Res. Bull. 100 (2018) 322–332.
[44] A.R. Ribeiro, M. Pedrosa, N.F.F. Moreira, M.F.R. Pereira, A.M.T. Silva, Environmental friendly method for urban wastewater monitoring of micropollutants defined in the Directive 2013/39/EU and Decision 2015/495/EU, J. Chromatogr. A 1418 (2015) 140–149.
[45] M.J. Lima, A.M.T. Silva, C.G. Silva, J.L. Faria, Graphitic carbon nitride modified by thermal, chemical and mechanical processes as metal-free photocatalyst for the selective synthesis of benzaldehyde from benzyl alcohol, J. Catal. 353 (2017) 44–53.
[46] P. Wu, J. Wang, J. Zhao, L. Guo, F.E. Osterloh, Structure defects in g-C_3N_4 limit visible light driven hydrogen evolution and photovoltage, J. Mater. Chem. A 2 (2014) 20338–20344.
[47] Y. Zhang, A. Thomas, M. Antonietti, X. Wang, Activation of carbon nitride solids by protonation: morphology changes, enhanced ionic conductivity, and photoconduction experiments, J. Am. Chem. Soc. 131 (2009) 50–51.
[48] D. Fatta-Kassinos, M.I. Vasquez, K. Kümmerer, Transformation products of pharmaceuticals in surface waters and wastewater formed during photolysis and advanced oxidation processes – degradation, elucidation of byproducts and assessment of their biological potency, Chemosphere 85 (2011) 693–709.
[49] E. Lee, H.K. Shon, J. Cho, Role of wetland organic matters as photosensitizer for degradation of micropollutants and metabolites, J. Hazard. Mater. 276 (2014) 1–9.
[50] H. Xu, W.J. Cooper, J. Jung, W. Song, Photosensitized degradation of amoxicillin in natural organic matter isolate solutions, Water Res. 45 (2011) 632–638.
[51] M. Rumi, J.W. Perry, Two-photon absorption: an overview of measurements and principles, Adv. Opt. Photon. 2 (2010) 451–518.
[52] N.F.F. Moreira, C.A. Orge, A.R. Ribeiro, J.L. Faria, O.C. Nunes, M.F.R. Pereira, A.M.T. Silva, Fast mineralization and detoxification of amoxicillin and diclofenac by photocatalytic ozonation and application to an urban wastewater, Water Res. 87 (2015) 87–96.
[53] M. Bosio, S. Satyro, J.P. Bassin, E. Saggioro, M. Dezotti, Removal of pharmaceutically active compounds from synthetic and real aqueous mixtures and simultaneous disinfection by supported TiO_2/UV-A, H_2O_2/UV-A, and TiO_2/H_2O_2/UV-A processes, Environ. Sci. Pollut. Res. - Int. (2018).
[54] C.S. Uyguner-Demirel, N.C. Birben, M. Bekbolet, Elucidation of background organic matter matrix effect on photocatalytic treatment of contaminants using TiO_2: a review, Catal. Today 284 (2017) 202–214.
[55] J. Schneider, M. Matsuoka, M. Takeuchi, J. Zhang, Y. Horiuchi, M. Anpo, D.W. Bahnemann, Understanding TiO_2 photocatalysis: mechanisms and materials, Chem. Rev. 114 (2014) 9919–9986.
[56] E. Colombo, M. Ashokkumar, Comparison of the photocatalytic efficiencies of continuous stirred tank reactor (CSTR) and batch systems using a dispersed micron sized photocatalyst, RSC Adv. 7 (2017) 48222–48229.
[57] S. Sarkar, C. Bhattacharjee, S. Sarkar, Studies on the performance of annular photo reactor (APR) for pharmaceutical wastewater treatment, J. Water Process. Eng. 19 (2017) 26–34.
[58] M.J. Sampaio, C.G. Silva, A.M.T. Silva, V.J.P. Vilar, R.A.R. Boaventura, J.L. Faria, Photocatalytic activity of TiO_2-coated glass raschig rings on the degradation of phenolic derivatives under simulated solar light irradiation, Chem. Eng. J. 224 (2013) 32–38.
[59] S. Arzate, J.L. García Sánchez, P. Soriano-Molina, J.L. Casas López, M.C. Campos-Mañas, A. Agüera, J.A. Sánchez Pérez, Effect of residence time on micropollutant removal in WWTP secondary effluents by continuous solar photo-Fenton process in raceway pond reactors, Chem. Eng. J. 316 (2017) 1114–1121.
[60] R.G. Nair, P.J. Bharadwaj, S.K. Samdarshi, Design improvement and performance evaluation of solar photocatalytic reactor for industrial effluent treatment, Ecotoxicol. Environ. Saf. 134 (2016) 301–307.
[61] M.A. Behnajady, N. Modirshahla, N. Daneshvar, M. Rabbani, Photocatalytic degradation of C.I. Acid Red 27 by immobilized ZnO on glass plates in continuous-mode, J. Hazard. Mater. 140 (2007) 257–263.
[62] N.F.F. Moreira, J.M. Sousa, G. Macedo, A.R. Ribeiro, L. Barreiros, M. Pedrosa, J.L. Faria, M.F.R. Pereira, S. Castro-Silva, M.A. Segundo, C.M. Manaia, O.C. Nunes, A.M.T. Silva, Photocatalytic ozonation of urban wastewater and surface water using immobilized TiO_2 with LEDs: micropollutants, antibiotic resistance genes and estrogenic activity, Water Res. 94 (2016) 10–22.